Analysis on Thrust Characteristics of Slotless Iron-Cored PMLSM According to PM Magnetization Patterns

Seok-Myeong Jang*, Dae-Joon You†, Sung-Ho Lee and Won-Bum Jang***

Abstract - The development of modern high-energy magnet materials has allowed the replacement of field coils in many different types of electromagnetic energy conversion machines. As well, the linear synchronous motor has recently been proposed for linear motion with high efficiency and thrust. Thus, this paper presents an analytical solution for the high thrust and cost reduction of the Iron-Cored Permanent Magnet Linear Synchronous Motor (PMLSM) considering magnetization arrays and geometry. Hence, the superior utilization points in each of the magnetization arrays are provided by the height ratio of the magnet/air-gap and magnet/winding coil, etc. In formulation, the space harmonic method in analytical solutions and the generalized 2-D tensor finite element analysis can be used to evaluate force components in magnetostatic devices including the magnetostrictive phenomenon.

Keywords: High thrust, PM magnetization patterns, Slotless iron-cored PMLSM

1. Introduction

Recently, Permanent Magnet Linear Synchronous Motors (PMLSMs) have become widely used throughout various applications including factory automation, transportation applications, and conveyance systems where their simplicity, high efficiency, linearity, and smooth, quiet operation are advantageous. Accordingly, there is a great amount of innovative design activity, in which there is pressure to improve the efficiency and the thrust and to reduce thrust ripple and noise caused by the detent force. In order to facilitate the design optimization and accurate dynamic modeling of linear permanent magnet machines, a variety of techniques have been employed to predict the magnetic field distribution. The most common approach is to use a lumped equivalent circuit. However, while this allows the relationship between critical design parameters and machine performance to be established analytically, it suffers from problems associated with accuracy, particularly when flux leakage is significant and the flux pathways are complex. With the availability of powerful software tools, numerical techniques such as finite element analysis provide an accurate means of determining the field distribution and saturation. They remain time-consuming and do not provide as much insight as analytical solutions into the influence of the design parameters on the machine behavior [1].

Therefore, in our presentation, a two-dimensional (2-D) analytical space harmonic solution according to magnetic field distribution was established in the rectangular coordinate system. Furthermore, in order to remove the detent force and improve the power efficiency, we present a slotless 3-phase stator with iron core and a mover with three types of magnetization patterns. For the analytical solution and motor geometry, we represent the optimal point due to magnetization arrays in applications with the high thrust density per magnet volume.

In good agreement with the specifications from the finite element method (FEM), the analytical results confirm the validity of the design and analysis.

2. Magnetic Field Analysis and Thrust

2.1 Analytical model due to PM magnetization patterns

In order to analyze linear PM electric machines effectively, we have adopted an approach that can treat both magnetized material and winding current during two-dimension analysis. Fig. 1 depicts the general frame for analysis of the linear synchronous motor with moving magnet type. In the linear synchronous motor model with a two-dimension rectangular frame, the upper region with height Δ represents the mover magnet array, carrying a rectangular coordinate frame (x', y', z') that is relatively displaced from the stator frame (x, y, z) by the vector $(\Gamma+x_o)\, i_x + z_o i_z$. Thus, x_0 is the motor air gap, and z_0 is the lateral displacement of the magnet array relative to the stator. The motor is

† Corresponding Author: Department of Electrical Engineering, Chungnam National University, Daejeon, 305-764, Korea (ydjgood@cnu.ac.kr)
* Department of Electrical Engineering, Chungnam National University, Daejeon, 305-764, Korea (smjang@cnu.ac.kr, wbjang@hanafos.com).
** LG Digital Appliance Lab., 327-23, Gasandong, Gumchun-gu, Seoul, Korea (iemechas@lge.com)
Received April 12, 2004 ; Accepted September 2, 2004

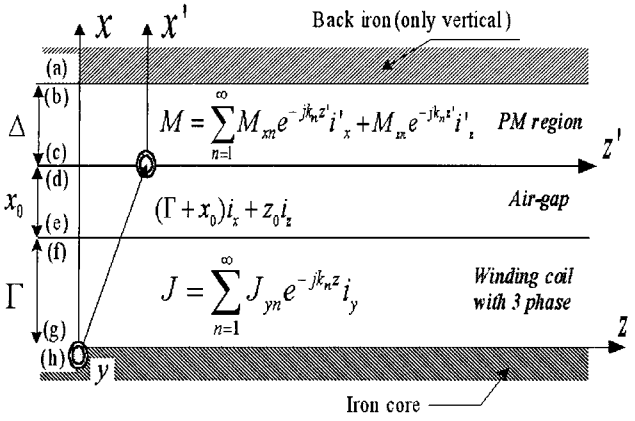

Fig. 1 Analysis model of linear synchronous Motor.

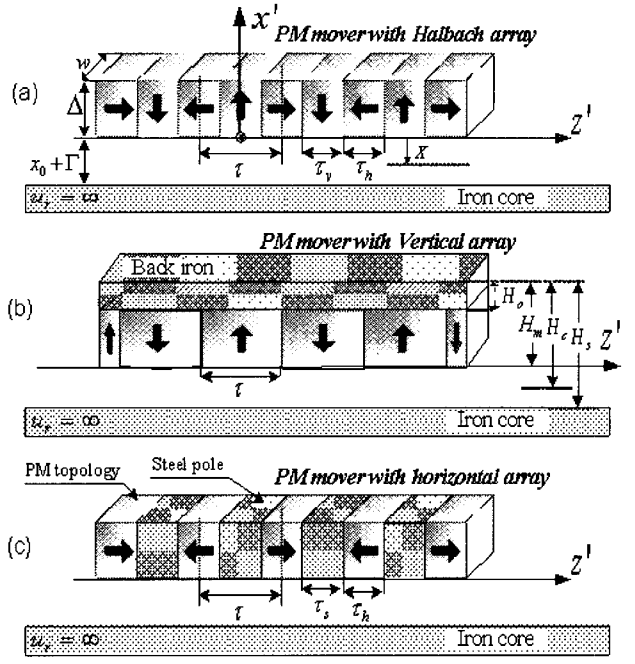

Fig. 2 PM magnetization patterns with iron core of stator: (a) Halbach magnetization (b) vertical magnetization (c) horizontal magnetization.

assumed to have a depth of w and *(a)-(h)* represent the surfaces at the indicated boundaries. Edge effects in the y-direction are ignored.

Fig. 2 shows four and a half pole magnetization patterns with: (a) Halbach magnetization array, (b) vertical magnetization array and (c) horizontal magnetization array considering width τ_v, τ_h of magnet topology and iron core [2]. Here, the pole pitch of the vertical array is defined by $\tau = \tau_v$ and the pole pitch of the horizontal array having steel-pole width τ_s is $\tau = \tau_h + \tau_s$ in the same PM volume. Also, the Halbach magnetization array has an inherently self-shielding property, and thereby doesn't require a back iron. Furthermore, the magnetic field of the horizontal array is influenced in the iron-core position.

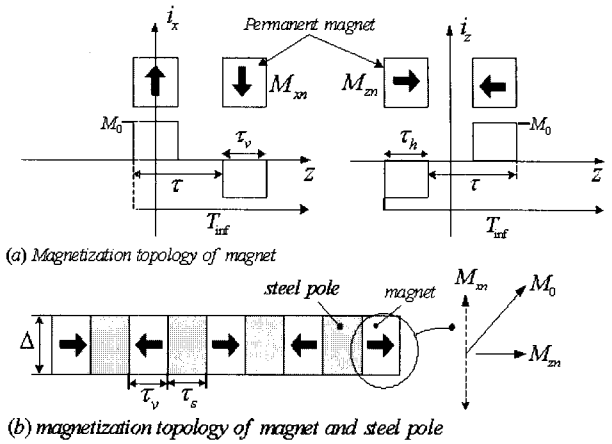

Fig. 3 Magnetization modeling according to magnet array.

2.2 Magnetic field by permanent magnet

The governing field equation inside the permanent magnet, in terms of the Coulomb gauge $\nabla \bullet A = 0$ is given by

$$\nabla^2 \vec{A} = -\mu_0 (\nabla \times \vec{M}) \tag{1}$$

where $\vec{A}$ is the magnetic vector potential, μ_0 denotes the free space permeability, and $\vec{M}$ is the magnetization of the permanent magnet. Magnetization by magnet topology with the Halbach array is represented by the infinite Fourier series both in vertical (x'-direction) and horizontal (z'-direction) magnetization components through terms M_{zn} and M_{xn}, respectively, as shown in Fig. 3, i.e.,

$$\begin{cases} M_{xn} = \sum_{n=1}^{\infty} \dfrac{2}{T_{\inf}} \int_{-\frac{\tau_v}{2}}^{2\tau-\frac{\tau_v}{2}} \pm M_0 e^{jk_n z} dz \\ M_{zn} = \sum_{n=1}^{\infty} \dfrac{2}{T_{\inf}} \int_{-\tau}^{\tau} \pm M_0 e^{jk_n z} dz \end{cases} \tag{2}$$

where the magnetization M is related to the remanence B_r by $M_0 = B_r/\mu_0$ [1]. Also, in the pitch of the magnet array for the infinite period, the spatial wave number of the n^{th} harmonic is $k_n = 2\pi n / T_{inf}$. Here, when the infinite period is identical to the motor period 2τ, the spatial wave number of the n^{th} harmonic is $k_n = 2\pi n / 2\tau$.

In case of the vertical topology represented in Fig. 2 (b), $M_{zn}=0$. Therefore, the vertical magnetization array only exists in M_{xn}. Also, in the horizontal array of Fig. 2 (c), the magnetization is influenced on the magnet height Δ and steel-pole τ_s as illustrated in Fig. 3 (b). The magnetization vector quantity of horizontal magnetization topology modeling by total M_0 can be expressed as

$$\begin{cases} |M_{xn}| = \dfrac{\Delta}{\sqrt{\Delta^2+\tau_s^2}} \dfrac{B_r}{\mu_0} \\ |M_{zn}| = \dfrac{\tau_s}{\sqrt{\Delta^2+\tau_s^2}} \dfrac{B_r}{\mu_0} \end{cases} \quad (3)$$

It is convenient to formulate the field distribution in terms of magnetic vector potential defined as $B = \nabla \times A$. In two-dimensional cases where the field lays in the *xz*-plane with no dependency on *y*, the vector potential is purely *y*-directed. In this case, the vector Poisson equation simplified to the scalar relationship is given as follows [3]:

$$\frac{\partial^2}{\partial y^2} A_y = -\mu_0 \left(\frac{\partial}{\partial z} M_x - \frac{\partial}{\partial x} M_z + J_y\right) \quad (4)$$

where M_x, M_z are magnetization components of the magnet array and J_y is the source of current density. However in the air space, the source is zero.

The homogeneous solution inside the magnet region with height Δ takes form according to the solution of the Laplace equation. Thus we obtain the transfer relations at the boundaries (b) and (c). The transfer relations are given by

$$\begin{bmatrix} B^{(b)}_{zn} \\ B^{(c)}_{zn} \end{bmatrix} = k_n \begin{bmatrix} \coth k_n\Delta & -1/\sinh k_n\Delta \\ 1/\sinh k_n\Delta & -\coth k_n\Delta \end{bmatrix} \begin{bmatrix} A^{(b)}_{yn} \\ A^{(c)}_{yn} \end{bmatrix} + \begin{bmatrix} \dfrac{\cosh k_n\Delta - 1}{\sinh k_n\Delta} \\ \dfrac{\cosh k_n\Delta - 1}{\sinh k_n\Delta} \end{bmatrix} [j\mu_0 M_{xn}] \quad (5)$$

In order to solve the field quantities, eight more independent equations are required. These are derived from the boundary conditions related to the field and the potential at each of the boundaries as presented in Fig. 1; these conditions are provided in Appendix A. Using these boundary conditions, the normal and tangential flux density at a free location X of the air-gap can be obtained as follows, respectively.

$$B^{(X)}_{xn} = \left(\frac{\mu_0 M_{xn}}{2} - \frac{j\mu_0 M_{zn}}{2}\right)(1-e^{-k_n\Delta})(e^{-2k_n(x_0+\Gamma)}e^{k_nX} + e^{-k_nX})e^{-jk_nz'}$$

$$B^{(X)}_{zn} = -\left(\frac{j\mu_0 M_{xn}}{2} + \frac{\mu_0 M_{zn}}{2}\right)(1-e^{-k_n\Delta})(e^{-2k_n(x_0+\Gamma)}e^{k_nX} - e^{-k_nX})e^{-jk_nz'} \quad (6)$$

In the case of vertical topology, the boundary condition is considered of back iron and no equivalent surface current density. Using these boundary conditions, flux density also can be obtained as follows, respectively.

$$B^{(X)}_{xn} = \frac{\mu_0 M_{xn}}{2}\left[\frac{(e^{2k_n\Delta}+e^{-2k_n\Delta}-2)(e^{-k_n(x_0+\Gamma)}e^{\gamma_nX}+e^{-k_n(x_0+\Gamma)}e^{-k_nX})}{(e^{2k_n\Delta}-1)e^{k_nx_0}+(e^{-2k_n\Delta}-1)e^{-k_nx_0}}\right]e^{-jk_nz'}$$

$$B^{(X)}_{zn} = \frac{-j\mu_0 M_{xn}}{2}\left[\frac{(e^{2k_n\Delta}+e^{-2k_n\Delta}-2)(e^{-k_n(x_0+\Gamma)}e^{k_nX}-e^{k_n(x_0+\Gamma)}e^{-X})}{(e^{2k_n\Delta}-1)e^{k_nx_0}+(e^{-2k_n\Delta}-1)e^{-k_nx_0}}\right]e^{-jk_nz'} \quad (7)$$

2.3 Magnetic field due to slotless iron-cored coil

The stator layer is of thicknessΓ, and within this layer the current density is represented by the infinite Fourier series.

$$J = \sum_{n=\infty}^{-\infty} J_{yn} e^{-jk_nz} i_y \quad (8)$$

where J_{yn} is the complex amplitude of the n^{th} current density component. Though a similar method as in the case of the magnet, we obtain the transfer relations inside the stator current.

$$\begin{bmatrix} B^{(f)}_{zn} \\ B^{(g)}_{zn} \end{bmatrix} = k_n \begin{bmatrix} \coth k_n\Gamma & -\dfrac{1}{\sinh k_n\Gamma} \\ \dfrac{1}{\sinh k_n}\Gamma & -\coth k_n\Gamma \end{bmatrix} \begin{bmatrix} A^{(f)}_{yn} \\ A^{(g)}_{yn} \end{bmatrix} - \begin{bmatrix} \dfrac{\cosh k_n\Gamma - 1}{\sinh k_n\Gamma} \\ \dfrac{\cosh k\Gamma_n - 1}{\sinh k_n\Gamma} \end{bmatrix} \begin{bmatrix} \dfrac{\mu_0}{k_n} J_{yn} \end{bmatrix} \quad (9)$$

Only vertical topology has a back iron. Therefore, two types for the current coil analysis model exist, iron and no iron. Using the boundary conditions considered of iron and back iron, in the current coil containing a mover of Halbach and horizontal array, the tangential and normal flux density at a free location X_c of the air-gap could be obtained as follows

$$B^{(Xc)}_{zn} = -\frac{\mu_0}{2\gamma_n} J_{yn}(1-e^{-2\gamma_n\Gamma})e^{-\gamma_nXc}$$

$$B^{(Xc)}_{xn} = \frac{j\mu_0}{2k_n} J_{yn}(1-e^{-2\gamma_n\Gamma})e^{-\gamma_nXc} \quad (10)$$

In the case of the current coil containing a mover of the vertical array, the magnetic fields at a free location of the air gap are

$$B^{(X_c)}_{zn} = \frac{\mu_0 J_{yn}}{2\gamma_n}(1-e^{2\gamma_n\Gamma})\left(\frac{e^{2\gamma_n(x_0+\Delta)}e^{-\gamma_nXc} - e^{\gamma_nXc}}{(e^{2\gamma_n(x_0+\Delta+\Gamma)}-1)}\right)$$

$$B^{(X_c)}_{xn} = \frac{j\mu_0 J_{yn}}{2k_n}(e^{2\gamma_n\Gamma}-1)\left(\frac{e^{2\gamma_n(x_0+\Delta)}e^{-\gamma_nXc} + e^{\gamma_nXc}}{(e^{2\gamma_n(x_0+\Delta+\Gamma)}-1)}\right) \quad (11)$$

2.4 Thrust by magnetic field

We describe the force for superposition of the flux

density due to the magnet and the stator excitation currents. This force is derived via the Maxwell stress tensor. The stress tensor T_{ij} for magnetically linear materials associated with the Korteweg-Helmholtz force density is given by [3]:

$$T_{ij} = \mu H_i H_j - \frac{\mu}{2} H_k H_k \tag{12}$$

The force acting on a volume of the magnet array is provided by the integral of the stress tensor over the surface of the volume. In this case, the components on the z-faces of the volume cancel due to symmetry. The only contribution is along the bottom surface, which we assume to lie on the boundary (d) in Fig. 1. If the lower surface encloses an integer number of periods and is of area $S = wl$, where pitch of the magnet l is 2τ, the z-directed thrust acting on the enclosed section of the magnet array is given by [3]

$$F_z = -S\left\langle T_{xz}^{(d)} \right\rangle_z = -S\mu_0 \left\langle H_x^{(d)} H_z^{(d)} \right\rangle_z \tag{13}$$

where the angle bracket expression $<\bullet>_z$ indicates the spatial average of the quantity enclosed by the brackets.

Table 1 Specifications of the Iron-cored PMLSM

Parameters	Values of Parameters	
Turns of Coil	150	(turns)
Pitch of Pole	51	(mm)
Length of Magnet	25	(mm)
Steel-Pole Length	25	(mm)
Height of Magnet	25	(mm)
Air Gap	5	(mm)
Height of Coil	6	(mm)
Dept of Motor	25	(mm)
Pole pairs of PM	2+1/4	
Max Current per Phase	1	(A)

3. Verification for analytical solution by FEM

Generally, the predicting and searching process of the optimal point is accompanied by an analytical solution. However, the examination of the data for accuracy is accomplished by FEM. As such, the specifications listed in Table I are for verification during analytical solutions. In order to analyze the iron-core PMLSM, we first study several possible magnet arrays and solve for their associated field as shown in Fig. 4. The result is that flux density of the Halbach topology is stronger by $\sqrt{\ }$ times than with the conventional array identical to the air-cored PMLSM. Also, the Halbach array does not require any ferromagnetic yoke. We next solved for the fields due to the stator winding as illustrated in Fig. 5. In the case of iron-cored PMLSM, the back iron of vertical topology has no effect on flux density due to current coil. Superposition is then applied to the fields in the presence of both the stator and the magnet mover. The thrust forces using Maxwell's stress tensor are separated in Fig. 6 into three types of magnet array. In the specifications listed in Table 1, thrust force of the Halbach magnetized motor is about 20(N), as shown in Fig. 6. It can be seen that the Halbach magnetized motor is higher than the conventional array in terms of energy efficiency.

4. Comparisons and Design Criteria for PM Magnetization Arrays

In Fig. 1, we represented H_0, H_m H_c and H_s etc. For fixed values of H_m and ratio of H_m/H_c, Fig. 7 shows the variations of the fundamental peak flux density at the air gap according to variation of H_0/H_m. It can be seen that over a certain ratio (0.8) of H_o/H_m, the vertical array is superior to the Halbach array, and on conditions below a ratio (0.8), the Halbach array is superior to the others in terms of magnetic flux density. Also, below a ratio of (0.3), the horizontal array is slightly superior to the vertical array.

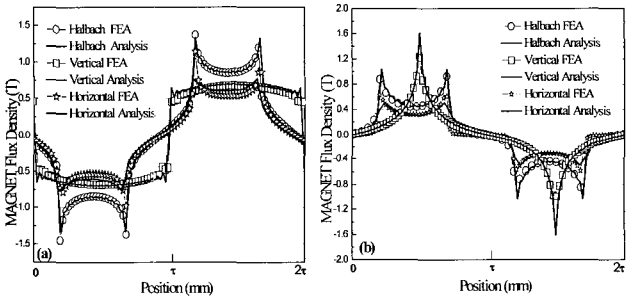

Fig. 4 The magneto-static flux density at the lower magnet surface (d) due to PM magnetization patterns with iron (a) x-directed flux density (b) z-directed flux density.

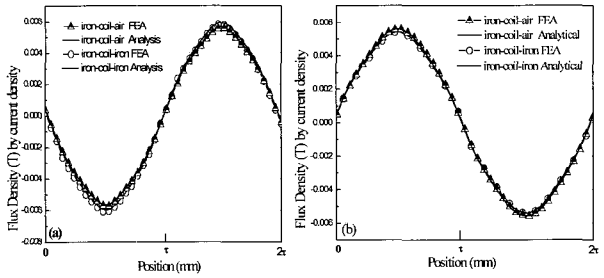

Fig. 5 The magneto-static flux density at the lower magnet surface due to 3-phase slotless current coil with steel (a)z-directed flux density (b)x-directed flux density

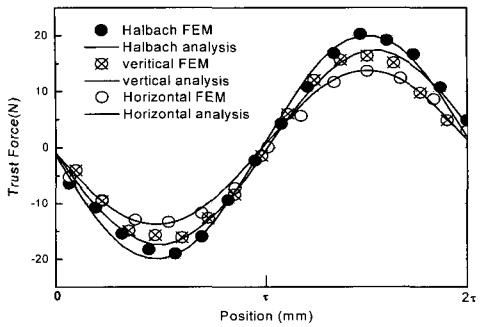

Fig. 6 FEM verification on thrust analysis according to PM magnetization array

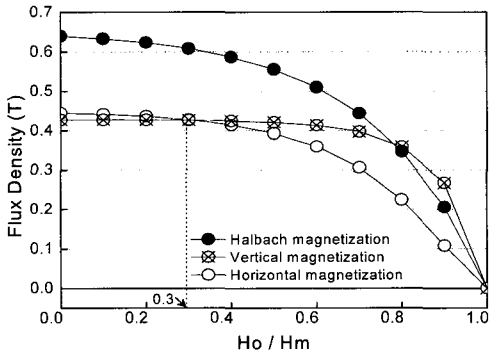

Fig. 7 Variation of the peak flux density at the air-gap with magnet thickness. (H_m =60(mm), H_m/H_c=0.95).

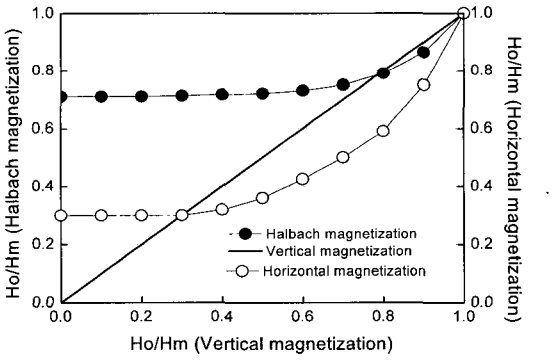

Fig. 8 Variation of H0/Hm for Halbach array and the horizontal array with H0/Hm of vertical array. (H_m/H_c=0.95, τ/H_s =0.72).

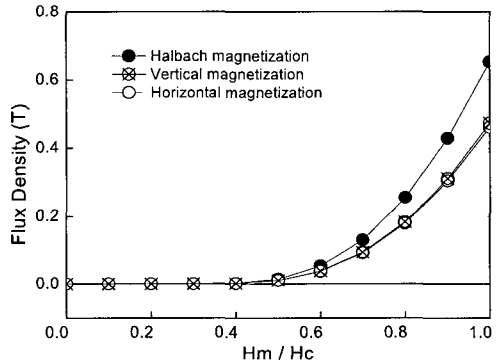

Fig. 9 Variation of peak flux density at the air-gap with magnetic air-gap (H_0/H_m=0.4).

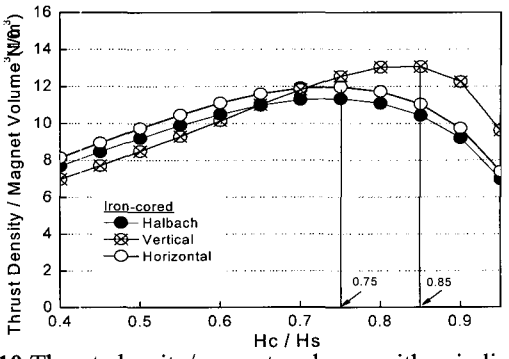

Fig. 10 Thrust density/magnet volume with winding coil thickness (H_m/H_c=0.95, copper loss=5(W)).

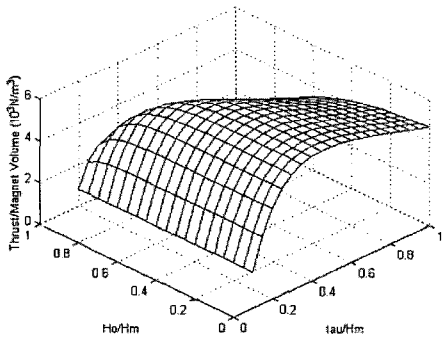

(a) Halbach magnetization array.

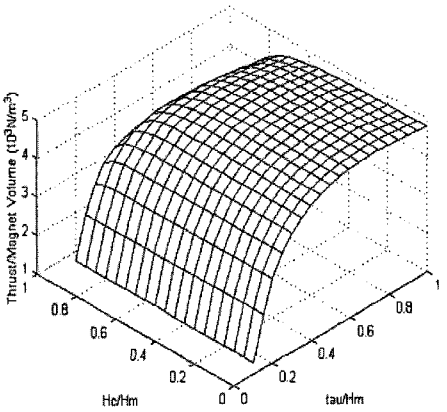

(b) Vertical magnetization array.

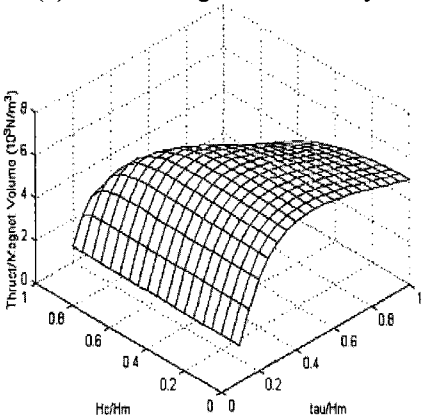

(c) Horizontal magnetization array.

Fig. 11 Variation of thrust density/magnet volume with H_0/H_m and τ/H_s (H_m=50(mm)).

Hence, in the application component, we can be aware of the utilizing point of magnet volume as shown in Fig. 8. For generating the identical magnet flux, Fig. 8 presents the variation of H_0/H_m in magnet volume of the equivalently required Halbach and horizontal array according to variation of H_0/H_m for vertical array.

Furthermore, for fixed values of ratio of H_0/H_m, Fig. 9 indicates the variations of the peak flux density at the air gap according to H_m/H_c. The decreasing amount of the magnet flux density according to increasing air gap is similar to the three array patterns. But we can see that over a certain ratio (0.4) of H_m/H_c, the Halbach array is superior to the others.

In Fig. 10, for fixed values of H_m/H_c and the copper loss of coil, the Fig. presents that the maximum thrust density/magnet volume with winding coil thickness exists. It can be seen that the maximum point of thrust density/volume of the vertical and horizontal magnetization array with H_c/H_s is superior to that of the Halbach array. But the vertical and horizontal array includes the back iron and steel pole. Hence, we can estimate that the Halbach array considering only the magnet is large at the maximum point.

Fig. 11 presents the variation of thrust density/magnet volume with H_0/H_m *and* τ/H_m for fixed values of H_m. It can be seen that the Halbach array (a) and the horizontal array (c) exist in the maximum point of thrust density/magnet volume with τ/H_m. But the vertical array (b) indicates that the thrust density/magnet volume with τ/H_m gradually slows down.

5. Conclusion

This paper has presented the design criteria of magnetization array patterns (Halbach, vertical, horizontal) utilizing linear synchronous permanent magnet motors. Generally, the design of a Cartesian linear motor has been developed in depth, and we are already familiar with the fact that the Halbach magnetization array field is a factor of $\sqrt{2}$ stronger than that of a conventional magnet array [4].

However, the magnetization arrays used for the motor mover are selected according to the geometry of each relation as well as the magnet and coil height, air gap, and pole length, etc. In particular, the characteristics of each array such as back-iron, steel pole, and self-shielding have greatly influenced the selection of the motor mover. In addition, from the viewpoint of cost reduction and efficiency, the thrust density/magnet volume indicates the accuracy of the selection base. The insight obtained from studying the design criteria on the magnetization array patterns may be beneficially used throughout other applications as well as in the case of the linear synchronous motor.

Acknowledgements

This work was financially supported by MOCIE through the IERC program, Korea.

Appendix A

Transfer relation of the air gap with height x_0 are given by (5) containing no source. In boundary of Fig. 1 for solving the transfer relation, we present that the bounded space at (a) and (d) composed by air in all space are half infinite. It is obtained by the transfer relations for the half-infinite regions above the surface (a) and below the surface (d), i.e.

$$B^{(a)}_{zn} = -k_n A^{(a)}_{yn}$$
$$B^{(d)}_{zn} = -k_n A^{(d)}_{yn}$$

Since there is no impulse of field everywhere, the vector potential is continuous at the boundary and the boundary condition for magnetic flux density by equivalent surface current density at the boundary (b) and (c) are [3], [4]

$$A^{(a)}_{yn} = A^{(b)}_{yn}$$
$$A^{(c)}_{yn} = A^{(d)}_{yn}$$
$$B^{(a)}_{zn} - B^{(b)}_{zn} = -\mu_0 M_{zn}$$
$$B^{(c)}_{zn} - B^{(d)}_{zn} = \mu_0 M_{zn}$$

Also, we assume that permeability $\mu_s = \infty$ of iron can be derived from

$$B^{(g)}_{zn} = 0$$
$$B^{(a)}_{zn} = 0 \quad \text{(In case of vertical array)}$$

References

[1] I. Boldea and S. A. Nasar, "Linear Electric Actuators and Generators. Cambridge", U.K.: Cambridge Univ. Press, 1997.

[2] Seok-Myeong Jang and Sung-Ho Lee, "Comparison of two types of PM linear synchronous servo and miniature motors with air-cored film Coils", IEEE

Trans. Magn., vol. 38, No. 5, pp. 3264-3266, Sept. 2002.
[3] David L. Trumper, Won-Jong Kim, and Mark E. Williams, "Design and analysis framework for linear permanent-magnet machines", IEEE Trans. Magn., vol. 32, No. 2, pp. 371-379, March/April. 1996.
[4] David L. Trumper and Mark E. Williams, "Halbach arrays in precision motion control", the Art and Science of Magnet Design. Vol. 1, Feb. 1995.

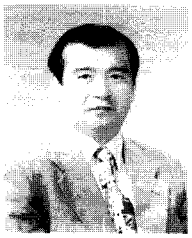

Seok-Myeong Jang
He was born in Korea in 1949. He received his B.E, M.S., and Ph.D. degrees from Hanyang University in 1976, 1978, and 1986, respectively. He is currently a Professor in the Department of Electrical Engineering, Chungnam National University. He worked as a Visiting Researcher in the Department of Electrical Engineering, Kentucky University in 1989. He is a member of KIEE. His fields of interest include the Design and Application of Linear Machines, High Speed Machines, and Linear Oscillating Actuators.
Tel: +82-42-821-5658

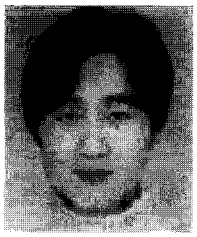

Dae-Joon You
He was born in Korea in 1976. He received his B.S. and M.S. degrees in Electrical Engineering from Chungnam National University in 2003 and 2005. He is currently working toward his Ph.D. degree in the Dept. of Electrical Engineering at Chungnam National University. His primary research interest is the design and control of PM linear machines.
Tel: +82-42-822-4933

Sung-Ho Lee
He was born in Korea in 1971. He received his B.S., M.S. and Ph.D. degrees in Electrical Engineering from Chungnam National University in 1997, 1999 and 2003, respectively. His research interests include the design and analysis of linear machines and automatic electric machine performance monitoring. He has previously been employed at the LG D/A Research Lab.
Tel: +82-42-822- 4933

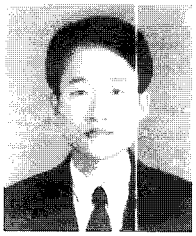

Won-Bum Jang
He was born in Korea in 1962. He received his B.S. and M.S. degrees in the Department of Electrical Engineering from Hanyang University in 1986 and 1988, respectively. His primary research interest is the drive and dynamic simulation of linear machines. He has previously been employed at ADD.
Tel: +82-42-821-2670 E-mail: